Electronic Supplementary Material (ESI) for Reaction Chemistry & Engineering.

Electronic supplementary information (ESI)

Hierarchical silica monoliths with submicron macropores as continuous-flow microreactors for reaction kinetic and mechanistic studies in heterogeneous catalysis

Richard Kohns,[a,b,1] Christian P. Haas,[a,1] Alexandra Höltzel,[a] Christian Splith,[b]
Dirk Enke[b] and Ulrich Tallarek[a,*]

[a] Department of Chemistry, Philipps-Universität Marburg, Hans-Meerwein-Strasse 4, 35032 Marburg, Germany

[b] Institute of Chemical Technology, Universität Leipzig, Linnéstrasse 3, 04103 Leipzig, Germany

[1] Both authors contributed equally to this work.

* Corresponding author.

Phone: +49-6421-28-25727; fax: +49-6421-28-27065; e-mail: tallarek@staff.uni-marburg.de.

Table S1 Results of the elemental analysis for sample Urea-7 after hydrothermal treatment, after calcination, as well as after functionalization.

	After hydrothermal treatment[a]	After calcination	After functionalization
N [%]	0	0.06	0.76
C [%]	12.40	0.29	5.58
H [%]	2.793	0.186	0.898

[a] After hydrothermal treatment, the sample was washed several times with water (until the pH of the aqueous solution became neutral) and then dried under reduced pressure.

All elemental analyses were performed by the "Gerätezentrum für Massenspektrometrie und Elementaranalytik" at the Department of Chemistry, Philipps-Universität Marburg (Marburg, Germany), using the CHN(S)-analyzer vario MICRO cube (Elementar Analysensysteme, Hanau, Germany). The data suggest that all nitrogen containing molecules like urea or its decomposition products can be washed out already after hydrothermal treatment. During phase separation, urea and its decomposition products are therefore mainly in the aqueous phase; at least, they are not incorporated (and fixed) in the gelled silica-PEO system. After calcination, all organic residues are removed, so that the nitrogen content after functionalization can be exclusively attributed to the functionalization with aminopropyl groups on the silica surface.

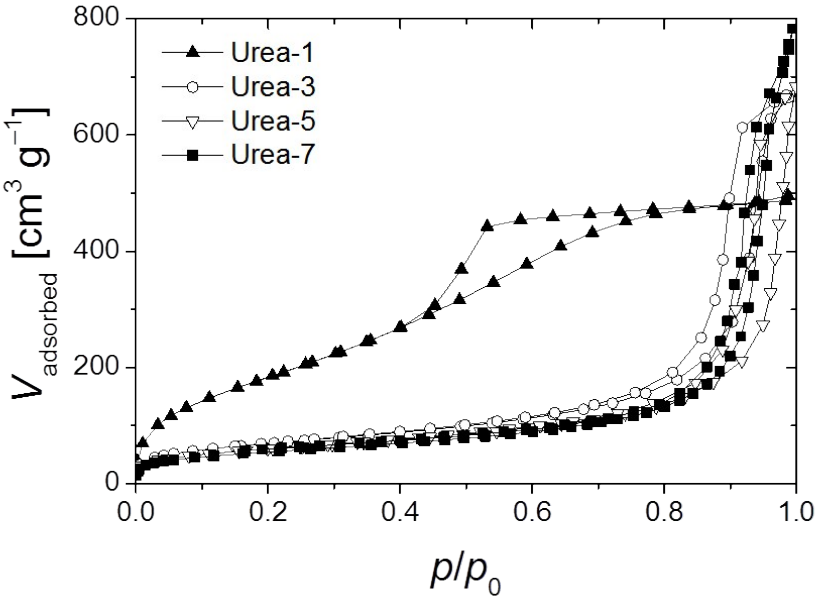

Fig. S1 Nitrogen sorption isotherms of the bimodal silica monoliths prepared with different urea content of the starting sol (cf. Table 1 in the main text).

Isotherms in Figure S1 can be classified as Type IV isotherms.[S1] Sample Urea-1 has a hysteresis Type H2(a); a saturation plateau is reached and the hysteresis closes again at $p/p_0 = 0.42$. The other samples show a Type H1 hysteresis. Here, the saturation plateau is not completely reached, which indicates incomplete filling of the pores. The change of hysteresis can be explained by the extent of mesopore widening during hydrothermal treatment, which depends on the urea content of the starting sol.

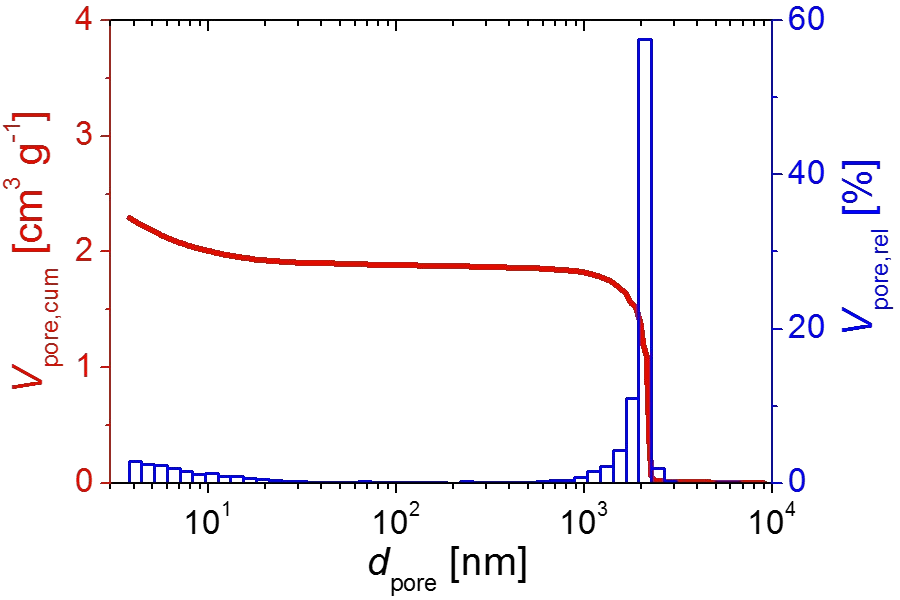

Fig. S2 Results of the MIP analysis (mercury intrusion curve and the derived pore size distribution as cumulative and relative pore volume, respectively) for sample Urea-1 (cf. Table 1 in the main text).

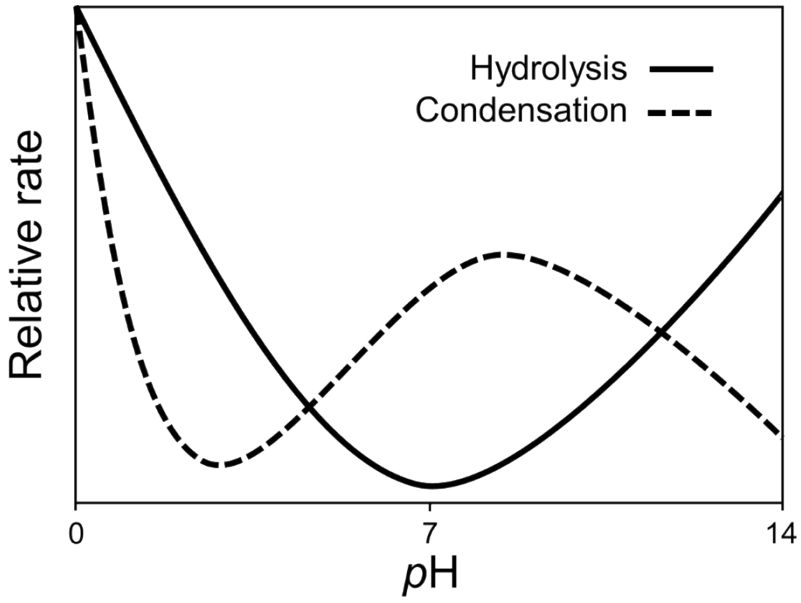

Fig. S3 pH dependence of hydrolysis and condensation rates in silicates. Adapted with permission from ref. S2. Copyright 1989 The American Association for the Advancement of Science.

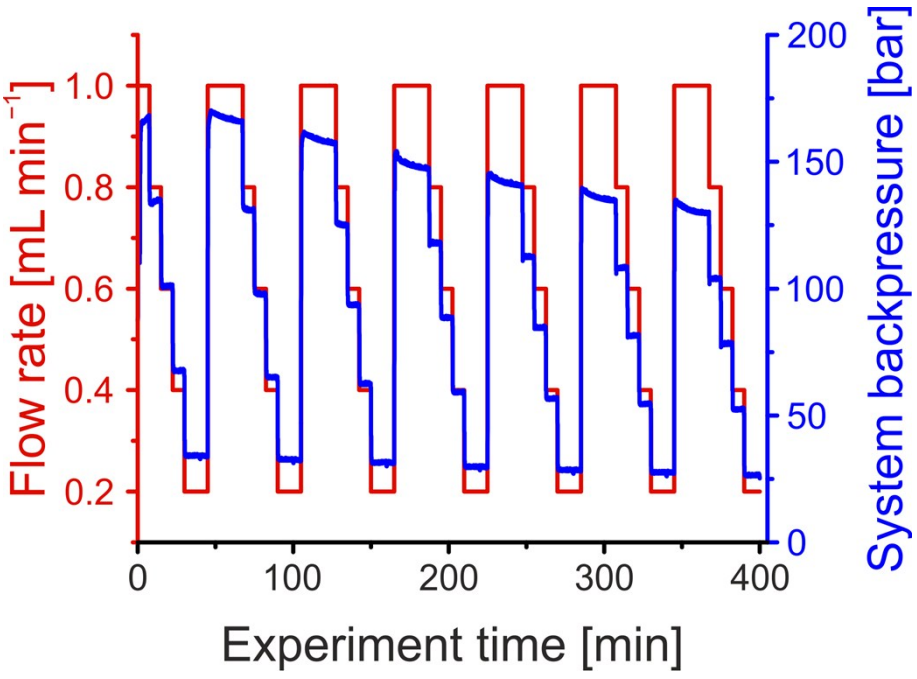

Fig. S4 Adjustments of volumetric flow rate by the quaternary pump and resulting backpressure in the flow-chemistry system with integrated microreactor (cf. Figure 8 in the main text, left half of the entire setup).

Estimation of the Thiele modulus for the silica monolithic microreactor

The Thiele modulus Φ accounts for the competition between the Knoevenagel reaction at the aminopropylated silica surface (represented by the rate constant k) and the limitation of transport of the reactant ECA by diffusion in the mesoporous skeleton of the monolith (represented by the effective diffusion coefficient D_{eff}):

$$\Phi = L_{skel}\sqrt{\frac{k}{D_{eff}}} = \frac{V_{skel}}{A_{ext}}\sqrt{\frac{k}{D_{eff}}} \qquad \text{(S1)}$$

The characteristic diffusion length L_{diff} is generally defined through the volume-to-surface ratio of the spatial domain, in which diffusion-limited transport takes place. In this study, $L_{skel} \equiv L_{diff}$ in eqn (S1) refers to diffusive transport in the mesopores of the silica skeleton (the white-appearing skeleton of the silica monoliths seen, for example, in Figure 5 of the main text, contains a fine network of mesopores; the macropores, by contrast, in which liquid flow occurs through the silica monolith, are outside this skeleton).

We have shown earlier[S3] that L_{skel} can be estimated from d_{skel} (the thickness of the typical worm-like silica skeleton in a monolith) by using the characteristic length parameter of a cylindrical pellet shape. Here, $d_{skel}/2$ corresponds to the radius of the assumed cylindrical (worm-like) structural element and the diffusion length then is one half of the cylinder radius:[S4]

$$L_{skel} = \frac{d_{skel}}{2}\cdot\frac{1}{2} = 0.11\ \mu m \qquad \text{(S2)}$$

(Before continuing, it has to be realized that, due to the very fine morphology of the monolith, the characteristic diffusion length in its mesoporous skeleton is on the order of only 100 nanometers, as illustrated with eqn (S2).)

For calculation of D_{eff} in eqn (S1) we first estimate the size of ECA, which is ~0.7 nm. Regarding hindered diffusion of this molecule in the mesoporous skeleton of the monolith, we notice that the ratio of ECA-size to the mean mesopore size in sample Urea-7 (d_{meso} = 25 nm) is as low as 0.028. We can thus simplify the general formula derived for hindered diffusion of finite-size tracers in mesoporous silica[S5] to that for point-like tracers [see, for example, eqn (10) with $\lambda = d_{tracer}/d_{meso}$ =

0 in S.-J. Reich, A. Svidrytski, D. Hlushkou, D. Stoeckel, C. Kübel, A. Höltzel and U. Tallarek, Hindrance factor expression for diffusion in random mesoporous adsorbents obtained from pore-scale simulations in physical reconstructions. *Ind. Eng. Chem. Res.*, 2018, **57**, 3031–3042.]:

$$D_{eff} = D_m \frac{\varepsilon_{meso}}{\tau_{meso}} \tag{S3}$$

In eqn (S3), ε_{meso} and τ_{meso} denote the porosity and diffusive tortuosity of the mesopore space accessible to point-like tracers, and D_m is the diffusion coefficient in the bulk liquid. Intraskeleton porosity for sample Urea-7 is $\varepsilon_{meso} = 0.69$ (given in Table 1 of the main text). For a very similar porosity (0.70) and mesopore size (25.7 nm), diffusion simulations in reconstructed mesoporous silica from these monoliths gave a diffusive tortuosity for point-like tracers of $\tau_{meso} = 1.35$[S5] [cf. the data for sample Si26 in Table 3 in S.-J. Reich, A. Svidrytski, D. Hlushkou, D. Stoeckel, C. Kübel, A. Höltzel and U. Tallarek, *Ind. Eng. Chem. Res.*, 2018, **57**, 3031–3042.]. The (electron tomographic) reconstruction employed in these diffusion simulations has been received from the mesoporous skeleton of such silica monoliths and should therefore be regarded as a very realistic structural model.

After having derived/collected values for L_{skel} (0.11 μm), ε_{meso} (0.69), and τ_{meso} (1.35), we now estimate the value for D_m using the Wilke–Chang equation[S6] applied to ECA in pure ethanol. The Wilke–Chang equation describes the molecular diffusion coefficient D_{AB} for the solute ECA (subscript A) in the solvent ethanol (subscript B) as:

$$D_{AB} = 7.4 \cdot 10^{-8} \frac{(\varphi_B M_B)^{0.5} T}{V_{b,A}^{0.6} \mu_B} \tag{S4}$$

For the solvent, φ_B is the association factor, M_B the molar mass, and μ_B the dynamic viscosity, whose temperature-dependence can be approximated as:[S7]

$$\mu_B(T) = \exp\left(-6.21 + \frac{1614}{T} + 0.00618\,T - 1.132 \cdot 10^{-5}\,T^2\right) \tag{S5}$$

The molar volume at the normal boiling point $V_{b,A}$ can be derived using the critical volume $V_{c,A}$, critical temperature $T_{c,A}$, boiling point $T_{b,A}$, and acentric factor ω_A of the solute ECA:[S8]

$$V_{b,A} = 7.047345 + 0.4\,V_{c,A} + \left(0.01724 + \frac{15.3765}{T_{c,A}} + 0.004387\,\omega_A\right)T_{b,A} \quad \text{(S6)}$$

All required thermophysical data for ECA can be found in the literature.[S9] They are summarized in Table S2 together with the resulting molar volume at the normal boiling point.

Table S2 Thermophysical properties of ethyl cyanoacetate (ECA).

$V_{c,A}$ [mL mol^{-1}]	$T_{c,A}$ [K]	$T_{b,A}$ [K]	ω_A [–]	$V_{b,A}$ [mL mol^{-1}]
358.00	679.00	482.20	0.426	170.38

Returning to the Wilke–Chang equation, the ECA diffusion coefficient at different temperatures was estimated using the association factor of $\varphi_B = 1.5$ and a molar mass of $M_B = 46.07$ g mol^{-1} for the solvent ethanol. The experimental values for the reaction rate constant k were determined in the temperature range $T = 10$–40 °C in steps of 5 °C. All temperature dependent values (including the targeted Thiele moduli) are summarized in Table S3.

Table S3 Ethanol viscosity, molecular and effective intraskeleton diffusion coefficients of ECA, as well as the rate constants of the rate-determining step in the Knoevenagel condensation, and the resulting Thiele moduli in the temperature range of 10–40 °C.

T [K]	μ_B [cPa]	D_{AB} [m^2 s^{-1}]	D_{eff} [m^2 s^{-1}]	k [s^{-1}]	Φ [–]
283.15	1.39	5.72×10^{-10}	2.92×10^{-10}	2.50×10^{-3}	0.00032
288.15	1.26	6.44×10^{-10}	3.29×10^{-10}	3.00×10^{-3}	0.00033
293.15	1.14	7.22×10^{-10}	3.69×10^{-10}	3.42×10^{-3}	0.00033
298.15	1.04	8.08×10^{-10}	4.13×10^{-10}	4.04×10^{-3}	0.00034
303.15	0.95	9.01×10^{-10}	4.61×10^{-10}	4.53×10^{-3}	0.00035
308.15	0.87	1.00×10^{-9}	5.11×10^{-10}	4.97×10^{-3}	0.00034

313.15	0.79	1.11×10^{-9}	5.67×10^{-10}	5.64×10^{-3}	0.00035

Since the Thiele moduli in the reaction system are on the order of 10^{-4}, mass transfer limitations can be safely excluded. It means that the entire surface is practically instantaneously available, without delay, reflecting highest effectiveness (i.e., an effectiveness factor of unity).

References

S1 M. Thommes, K. Kaneko, A. V. Neimark, J. P. Olivier, F. Rodriguez-Reinoso, J. Rouquerol and K. S. W. Sing, *Pure Appl. Chem.*, 2015, **87**, 1051–1069.

S2 D. W. Schaefer, *Science*, 1989, **243**, 1023–1027.

S3 C. P. Haas, T. Müllner, R. Kohns, D. Enke and U. Tallarek, *React. Chem. Eng.*, 2017, **2**, 498–511.

S4 M. E. Davis and R. J. Davis, *Fundamentals of Chemical Reaction Engineering*, McGraw-Hill, New York, NY, 2003, Chapter 6.3.

S5 S.-J. Reich, A. Svidrytski, D. Hlushkou, D. Stoeckel, C. Kübel, A. Höltzel and U. Tallarek, *Ind. Eng. Chem. Res.*, 2018, **57**, 3031–3042.

S6 C. R. Wilke and P. Chang, *AIChE J.*, 1955, **1**, 264–270.

S7 CHERIC, http://www.cheric.org/research/kdb/hcprop/cmpsrch.php.

S8 I. E. Maloka, *Pet. Sci. Technol.*, 2005, **23**, 133–136.

S9 C. L. Yaws, *Thermophysical Properties of Chemicals and Hydrocarbons*, William Andrew, Norwich, NY, 2014.